On the Relationships between Low-Frequency Variations of Earth's Rotation and Equatorial Atmospheric Angular Momentum

Tri Wahyu Hadi[1], Faiz Rohman Fajary[1], and Shigeo Yoden[2]

[1]Bandung Institute of Technology
[2]Institute for Liberal Arts and Sciences, Kyoto University, Kyoto, Japan

November 22, 2022

Abstract

This work mainly concerns low-frequency variations of Atmospheric Angular Momentum (AAM), emphasizing the role of the equatorial region and its relationships with the length of day LOD, whose observed time series indicate an accelerating Earth's rotation over the last several decades. We applied bivariate and trivariate Empirical Mode Decomposition methods to extract coherent nonstationary signals from the monthly time series of \$LOD\$ and the two components of AAM, i.e., the mass term M_Ω and the motion term M_r. It is found that, over the global domain, a decreasing trend of LOD during the last five decades correlates with an increasing trend in M_Ω, whereas the trend in M_r is negligible. However, there is a significantly positive trend in M_r of the equatorial lower troposphere (1000 to 700 hPa), which can be associated with a larger transfer of eastward momentum due to the accelerating Earth. Further analyses of spatio-temporal distribution of M_r anomalies suggest that, at multidecadal time scales, residual changes in the motion term of AAM across the globe tend to be in balance. The long-term positive trend in M_Ω, which is dominant over the equatorial latitude belt, is most likely attributed to prolonged effects of the global increase in surface pressure from the mid-1970s until the 1990s. Low-frequency variations of LOD are also found to have a high correlation with the Atlantic Meridional Oscillation index. Our results suggest that long-term changes in the Earth's rotation rate are partially attributable to the atmospheric and oceanic variability of comparable time scales.

On the Relationships between Low-Frequency Variations of Earth's Rotation and Equatorial Atmospheric Angular Momentum

T. W. Hadi[1], F. R. Fajary[1], S. Yoden[2]

[1]Atmospheric Science Research Group, Bandung Institute of Technology, Indonesia
[2]Institute for Liberal Arts and Sciences, Kyoto University, Japan

Key Points:

- A positive trend in the mass term of atmospheric angular momentum correlates with observed increasing rate of the Earth's rotation
- The conditions of accelerating Earth's rotation agree with a positive trend in the motion term of equatorial atmospheric angular momentum
- Interrelationship between low-frequency modulations of Earth's rotation and atmospheric angular momentum is evidenced

Corresponding author: Tri W. Hadi, `tri.wahyu@itb.ac.id`

Abstract

This work mainly concerns low-frequency variations of Atmospheric Angular Momentum (AAM), emphasizing the role of the equatorial region and its relationships with the length of day (LOD), whose observed time series indicate an accelerating Earth's rotation over the last several decades. We applied bivariate and trivariate Empirical Mode Decomposition methods to extract coherent nonstationary signals from the monthly time series of LOD and the two components of AAM, i.e., the mass term M_Ω and the motion term M_r. It is found that, over the global domain, a decreasing trend of LOD during the last five decades correlates with an increasing trend in M_Ω, whereas the trend in M_r is negligible. However, there is a significantly positive trend in M_r of the equatorial lower troposphere (1000 to 700 hPa), which can be associated with a larger transfer of eastward momentum due to the accelerating Earth. Further analyses of spatio-temporal distribution of M_r anomalies suggest that, at multidecadal time scales, residual changes in the motion term of AAM across the globe tend to be in balance. The long-term positive trend in M_Ω, which is dominant over the equatorial latitude belt, is most likely attributed to prolonged effects of the global increase in surface pressure from the mid-1970s until the 1990s. Low-frequency variations of LOD are also found to have a high correlation with the Atlantic Meridional Oscillation index. Our results suggest that long-term changes in the Earth's rotation rate are partially attributable to the atmospheric and oceanic variability of comparable time scales.

1 Introduction

The relationships between the variation of Earth's rotation rate — measured as changes in the length of day (LOD) — and climate have been a long-standing geophysical problem. The fact that the Earth has been spinning faster for the last several decades has also sparked attention from wider research communities and raised concerns about the possible effects of global warming. Numerous studies have previously confirmed that LOD excitations at intraseasonal, seasonal, to interannual time scales are associated with global atmospheric angular momentum (AAM) variations due to various climatic phenomena (Madden, 1987; Feldstein, 1999; Abarca-del Rio et al., 2000; Aoyama & Naito, 2000; Egger et al., 2007). However, attributions and physical mechanisms responsible for LOD variations at decadal or longer time scales are still a subject of scientific debates (e.g., Lambeck & Hopgood, 1982; Duhau, 2006; Barlyaeva et al., 2014; Huang et al., 2001).

The linkage between LOD and global atmospheric circulation has been deduced from the angular momentum conservation principle (Starr, 1948; Oort, 1989), but Gong et al. (2019) found that increasing global AAM in recent decades cannot explain the negative trend of LOD. Huang et al. (2001) have previously pointed out from climate simulations under global warming conditions that a positive trend in AAM should correspond to an increase in LOD by +0.3 to +0.5 ms in a century. In these works, the negative trends in LOD have been attributed to non-atmospheric sources, i.e., core-mantel (Gong et al., 2019) and postglacial (Huang et al., 2001) processes.

Thus, attributing low-frequency variations of LOD to climatic processes is still a challenging problem, but Zotov et al. (2016) pointed out a significant correlation between global temperature anomaly and LOD variations at a multidecadal time scale. This and some other studies suggest that dynamical interaction between climatic processes and Earth's rotation may also occur at decadal or longer time scales, which should be imprinted in the characteristics of the low-frequency variations of AAM. However, previous studies on the relationships between AAM and LOD variations may not have examined the following aspects in detail:

1. The total AAM is composed of two components expressed as $M_a = M_\Omega + M_r$ (e.g., Oort, 1989). The M_Ω term (herein, also referred to as the mass term) is the AAM component due to the Earth's solid body rotation, whereas the M_r term is due to atmospheric motion relative to the rotating Earth (hence, the motion term). It is important to note that M_Ω and M_r may undergo different time evolution as shown from the results of global warming simulations (Huang et al., 2001), which implies that correlations between M_Ω, M_r, and LOD need to be analyzed separately.
2. The AAM in the equatorial region has unique characteristics because M_Ω is large due to a relatively larger radius of the rotational plane. In addition, the zonal winds are predominantly easterly, so that M_r is on the average negative. The Earth's angular momentum conservation principle implies that the Earth's surface continuously transfers absolute angular momentum to the atmosphere along the equatorial latitudes with surface easterlies (Starr, 1948). The excess angular momentum in the equatorial atmosphere is then transported poleward mainly by weather processes in the troposphere to be deposited back to the Earth in midlatitudes with

surface westerlies (e.g., Weickmann & Sardeshmukh, 1994). The existence of Quasi-Biennial Oscillation (QBO) in the equatorial stratosphere also affects M_r variations (e.g., Salstein, 2015; Match & Fueglistaler, 2019).

3. Transient eddy momentum flux induced by phenomena like Madden-Julian oscillation (MJO) and El Niño southern oscillation (ENSO) in the tropical/equatorial region may leave a residual contribution to the mean climate state (Huang et al., 2001; Lee, 1999). However, MJO, ENSO, and other similar phenomena occur with irregular or quasi-regular patterns in time and space so that nonstationary variations likely characterize any residual signal.

The main objective of this study is to investigate low-frequency variations of global AAM and their relationships with LOD, with emphasis on the role of zonal-mean wind variations in the troposphere over the equatorial region. Technically, low-frequency components in a single time-series data can be extracted using several methods. The most common one is using a low-pass filter such as Butterworth filter design (e.g., Fajary et al., 2019). However, a novel approach is needed to extract coherent low-frequency signals from two or more nonstationary time series simultaneously. A data analysis method that can deal with nonstationary signals is empirical mode decomposition (EMD), which extracts intrinsic (natural) signals from an observed time series (Wu et al., 2007). Some implementations of EMD methods have been extended to multivariate inputs (e.g., Wu et al., 2016; Thirumalaisamy & Ansell, 2018). The application of multivariate EMD method allows us to analyze the correlations among M_Ω, M_r, and LOD simultaneously yet separately. Thus, besides a specific analysis of low-frequency variations in the equatorial AAM, we also emphasize the application of the multivariate EMD method as a novelty in the present work.

2 Materials and Methods

2.1 Data

In this investigation, we mainly analyze globally gridded monthly zonal winds from NCEP R1 reanalysis dataset (NCEP/NWS/NOAA/U.S. Department of Commerce, 1994; Kalnay et al., 1996) because, among others, it has the longest record spanning from 1948 to the present. We notice that there are biases in the NCEP data when compared to MERRA-2 reanalysis, which is considered as a benchmark for accuracy (Fujiwara et al., 2017), but we assume that long-term AAM variations are still well represented in the former dataset (Paek & Huang, 2012; Gong et al., 2019).

The LOD data, representing the Earth's rotation rate, was obtained from the International Earth Rotation and Reference Systems Service (IERS) as daily time series started from 1 January 1962 (IERS Earth Orientation Centre, 2020; Bizouard et al., 2019). In this work, we also use several climate indices accessible from the National Oceanic and Atmospheric Administration (NOAA) Physical Science Laboratory (PSL) website (PSL/NOAA, 2020). Herein, we mainly use monthly-mean time series; daily data are converted into monthly-mean time series through simple averaging. Any special treatment or data processing is explained in the text wherever needed for clarity. Additional results from our data processing can be found in the Supporting Information (SI).

2.2 Calculation of the AAM

The derivation of mathematical formulae to calculate AAM has been comprehensively discussed in previous works (Barnes et al., 1983; Salstein et al., 1993), and the globally integrated motion term can be expressed by (e.g., Gong et al., 2019; Huang et al., 2001)

$$M_r = \frac{a^3}{g} \int\limits_p \int\limits_\lambda \int\limits_\phi u \cos^2 \phi \, d\phi \, d\lambda \, dp, \tag{1}$$

whereas mass term is given by

$$M_\Omega = \frac{a^4 \Omega}{g} \int\limits_\lambda \int\limits_\phi p_s \cos^3 \phi \, d\phi \, d\lambda. \tag{2}$$

In these equations, u and p_s are zonal wind and surface pressure, respectively. For M_r, the integration is carried out with respect to latitude ϕ, longitude λ, and pressure p, whereas M_Ω is the horizontal integrals over the globe at the surface. The other parameters. i.e. Ω, a, and g are Earth's angular velocity, Earth's radius, and gravity acceleration assumed constant. There are two schemes for M_Ω calculation, i.e. with and without inverted barometric (IB) assumptions (Barnes et al., 1983; Salstein et al., 1993). In this case, we only applied a non-inverted barometric (non-IB) scheme in the evaluation of (2). We validated our results against AAM data provided by NOAA, which are also accessible from the aforementioned IERS's website. Although some discrepancies exists, comparisons of output variables show a linear correlation with regression coefficients close to unity (not shown).

2.3 Definition of The Equatorial Belt

In the following analyses, we differentiate the AAM variations contributed by the equatorial region from the global domain. Among quite a few literatures, Grimes (1951) define the equatorial belt by the latitudes between 15°S and 15°N where it is assumed that the Coriolis force ceases to predominate. Herein, we defines the equatorial belt by the latitudes between 20°S and 20°N where the climatology of AAM is predominantly negative as shown in Fig. S1(a) in SI. Although all-year negative AAM is mainly confined within the 15° latitudes, we consider to include transitional or buffer zones, where AAM may fluctuate between negative and positive values seasonally (Fig. S1(b)), so that our definition of the equatorial belt is wider than that of Grimes (1951) by 5°. Transition zones between the equatorial and mid-latitude regions are marked by a relatively rapid decrease of M_Ω with latitudes (Fig. S1(c)).

To our knowledge, there is no strict distinction between the definitions of equatorial and tropical belts, but it should be common sense to assume that the former is a subregion of the latter. The tropical belt itself has several definitions with latitudinal extents that may surpass 20° in both hemispheres depending on the metrics being used (Birner et al., 2014; Davis & Rosenlof, 2012). Egger and Hoinka (2005) used 27° latitudes to mark the boundaries between tropical and midlatitude regions when analyzing the characteristics of AAM. On the other hand, Huang et al. (2001) examined tropical contribution on changes in AAM due to projected increase in sea surface temperature (SST) under global warming conditions by averaging data between the latitudes of 13°S and 13°N. In the study, it is remarked that their index is not sensitive to the choice of the averaging domain.

2.4 Identification of Coherent Low-Frequency Variabilities

We employed the EMD method to analyze time-series data presumed to contain nonstationary low-frequency signals. A univariate EMD analysis of a time series $f(t)$ will result in its decomposition into several intrinsic mode functions, IMFs, i.e.,

$$f(t) = \sum_{n=1}^{N} IMF\#n(t) + \Re(t), \tag{3}$$

where $\Re(t)$ is the residual, the discrepancy between the summed IMFs and original time series. The EMD is a completely "data-driven" method because it does not assume any a priori basis function so that detection of spurious signals can be avoided (Wu et al., 2007). However, the maximum number of IMFs, N in Eq. (3), is determined through an iterative process with results that may be sensitive to small variations in the dataset. Consequently, each IMF obtained from EMD analysis of different time series may have different physical meanings and must be more carefully interpreted.

Various EMD techniques to analyze univariate and multivariate time series have also been developed and applied to climate data (e.g. Wu et al., 2016). In this work, we adopt the multivariate EMD method developed by Thirumalaisamy and Ansell (2018). By applying a multivariate EMD analysis, we assume that physically meaningful IMFs can be effectively rendered from correlated nonstationary time series. Matlab® codes to implement the multivariate EMD analysis have been provided by Thirumalaisamy (2020), which includes codes to perform simultaneous EMD with input up to 16 (channel) time series of one, two, and three spatial dimensions. For our purposes, however, it is sufficient to apply only bivariate and trivariate one-dimensional (either in latitude or pressure) EMD, whereby up to two or three time-series can be analyzed simultaneously in one code execution on a regular personal computer.

3 Results

3.1 Correlations between *LOD* and Global AAM

This subsection first discusses the correlation between LOD and two AAM components, i.e., M_r and M_Ω, computed over the global domain. From Fig. 1, we can see that the time series of LOD exhibit a decreasing trend from the 1970s to the present with superimposed oscillatory signals of multidecadal and shorter periods. It is also clear that M_Ω is two orders of magnitude larger than M_r, but the standard deviation of M_r is one order larger than that of M_Ω. However, it should be noted that M_r is always globally positive despite negative values in the equatorial region (further discussed below). In general, correlations between LOD and total AAM M_a are not visually discernible except for some concurrent spikes in certain years, such as that of 1982/83 El Niño. In addition, marked interdecadal variations can be seen in the time series of M_Ω, especially between the 1950s and 1980s.

Correlations among parameters in Fig. 1 are more intuitively depicted as scatter plots in Fig. 2. There is a positive correlation between M_r and LOD with a drift due

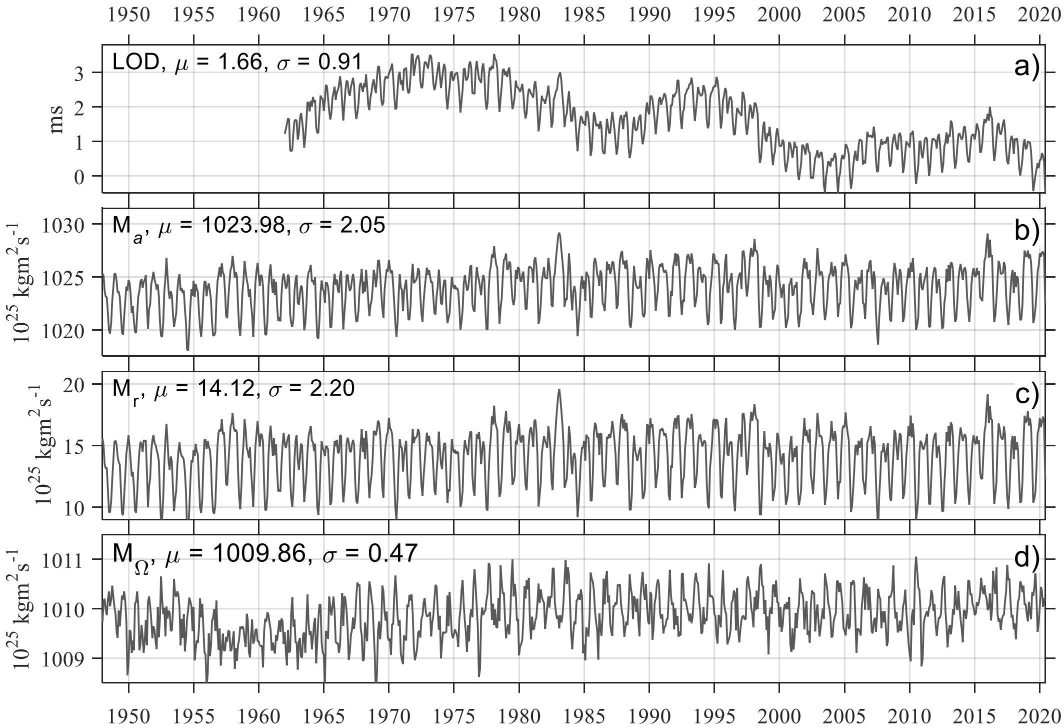

Figure 1. Time series of (a)LOD, (b)M_a, (c)M_r, and (d)M_Ω of the global AAM (see text for explanation) at a monthly time interval. Units, means μ, and standard deviations σ, of the time series are also indicated in the plots.

to the long-term decreasing trend of LOD, whereas M_Ω is negatively correlated with the other two parameters. We can see that the correlation patterns change over time by inspecting the color-coded time information, signifying a non-stationary relationship between compared parameters. The power spectral densities in Fig. 2(d) show that all parameters have strong and well-aligned annual and semiannual signals. Marked peaks are also identified at QBO (2.4-year) and ENSO (5.0-year) periods. Signals with longer periods are red-noise contaminated, and their peaks occur at different frequency bands.

We further investigate the correlations between LOD, M_r, and M_Ω by applying trivariate EMD analysis on the three time-series. Because all data have a very different range of values, each of the parameters is normalized as $\tilde{x} = (x - \mu_x)/\sigma_x$ where μ_x and σ_x are the mean and standard deviation of x. We found that the EMD analyses are also sensitive to the choice of window size, which is determined as a function of the distance between extrema in the signal (Thirumalaisamy & Ansell, 2018). In this case, we have chosen a window size equal to a maximum allowable value of 7 for all EMD analysis. Re-

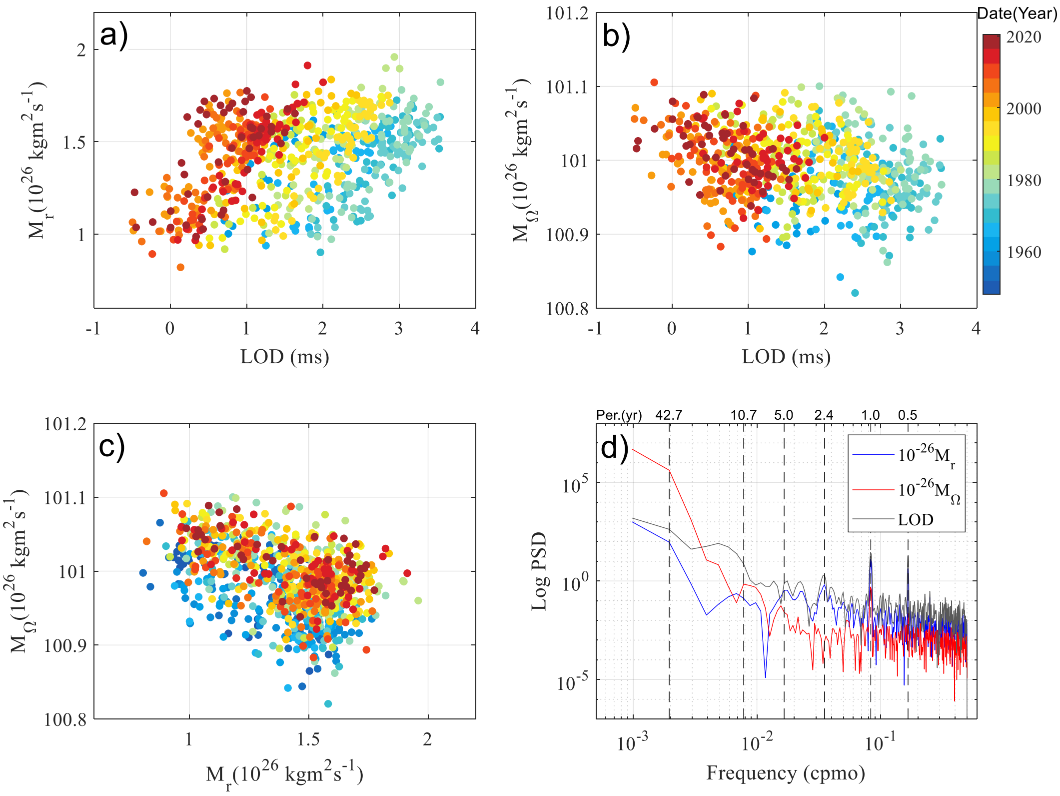

Figure 2. Scatter plots between parameters in Fig. 1 ((a) to (c)) and the corresponding Fourier power spectral densities (PSDs) in (d). Color codes are used to show time from the year 1948 to 2020. Values of M_r and M_Ω are multiplied by 10^{-26} prior to Fourier spectral computation.

sults of the EMD analysis are shown in Fig. 3 as scatter plots of the IMFs. In addition, to identify dominant periods in the decomposed signals, we also computed the cross power spectral density (CPSD) P_{xy} and Spearman's linear correlation coefficient r. The period associated with maximum CPSD is determined as the period T_{xy} of two correlated signals given in a time unit of month (abbreviated as "mo"). It should be noted that IMFs #1 and #2 mainly contain signals of sub-annual variations and are not shown in Fig. 3.

Consistent with the spectral analysis in Fig. 2, we can see that the strongest coherent signals are those of annual variation. However, there are two modes of annual variability represented by $IMF\#3$ and $IMF\#4$. Discontinuities (clustering of data) in $IMF\#3$ indicate the influence of strong seasonal patterns of midlatitude regions (see e.g., Salstein, 2015), whereas smoother $IMF\#4$ seems to characterize the contribution of tropical/equatorial region. Note that M_r and M_Ω are negatively correlated (r=-0.86) for $IMF\#3$, while those are not much correlated (r=-0.38) for $IMF\#4$. It can also be seen that M_r has a relatively stronger linear correlation with LOD, up to QBO (28 mo) time scale as indicated by the $IMF\#5$. On the other hand, correlations between M_Ω and LOD, as well as M_r, are much weaker except for $IMF\#3$. The results of EMD analysis clearly show that correlations between the three parameters become nonstationary at time scales of about 32 mo ($\approx$ 2.7 yr) and longer, especially when M_Ω is involved. In this EMD analysis, the three signals can be decomposed up to $IMF\#9$, but $IMF\#8$ is extremely weak and difficult to interpret.

We are particularly interested in $IMF\#9$ that represents signals with multidecadal time scales. Detailed temporal variations of $IMF\#9$ are shown in Fig. 4 along with the residuals, which are obtained by subtracting the summed IMFs from the original time series as defined by Eq. (3). In this case, the residual component $\Re(t)$ is a function with less than three detectable extrema and considered a non-oscillatory signal. Figure 4(a) clearly shows that the LOD contains relatively large oscillatory signals with periods of around 20 years, while M_r and M_Ω exhibit less well-defined oscillations at this time scale. It is of interest to note that variations in M_Ω show a relatively consistent phase against LOD with about five-year lag in the occurrences of local maxima. On the contrary, M_r variations have changed from out-of-phase, prior to the 1980s, to more in-phase after the 1990s. This explains the zero correlation coefficient between $IMF\#9$ of LOD and M_r, as shown in Figs. 3 and 4(a).

More comparable variations are depicted by the residuals of LOD and M_Ω in Fig. 4(b) where opposite long-term trends that dominate over weak fluctuations can be seen. The correlation coefficient computed from the time series of LOD and M_Ω in Fig. 4(b) is -0.72. On the other hand, the residual of M_r does not indicate a significant trend over the last five decades. These results are interesting because the AAM variations are basically more characterized by M_r rather than M_Ω, even under projected global warming conditions (e.g. Huang et al., 2001). Moreover, multidecadal variations of M_r and M_Ω in Fig. 4(a) are positively correlated (see, $IMFs\#9$ in Fig. 3, bottom right with r=0.57) in contrast to the negative correlations that characterize the annual variations in $IMFs$ #3 and #4. It is also of interest to note that such a positive correlation also characterizes $IMFs$ #6 and #7 with apparent contributions of ENSO and other variations of longer time scales. Considering that M_Ω is a function of $\cos^3\phi$ in Eq. (2), the equatorial re-

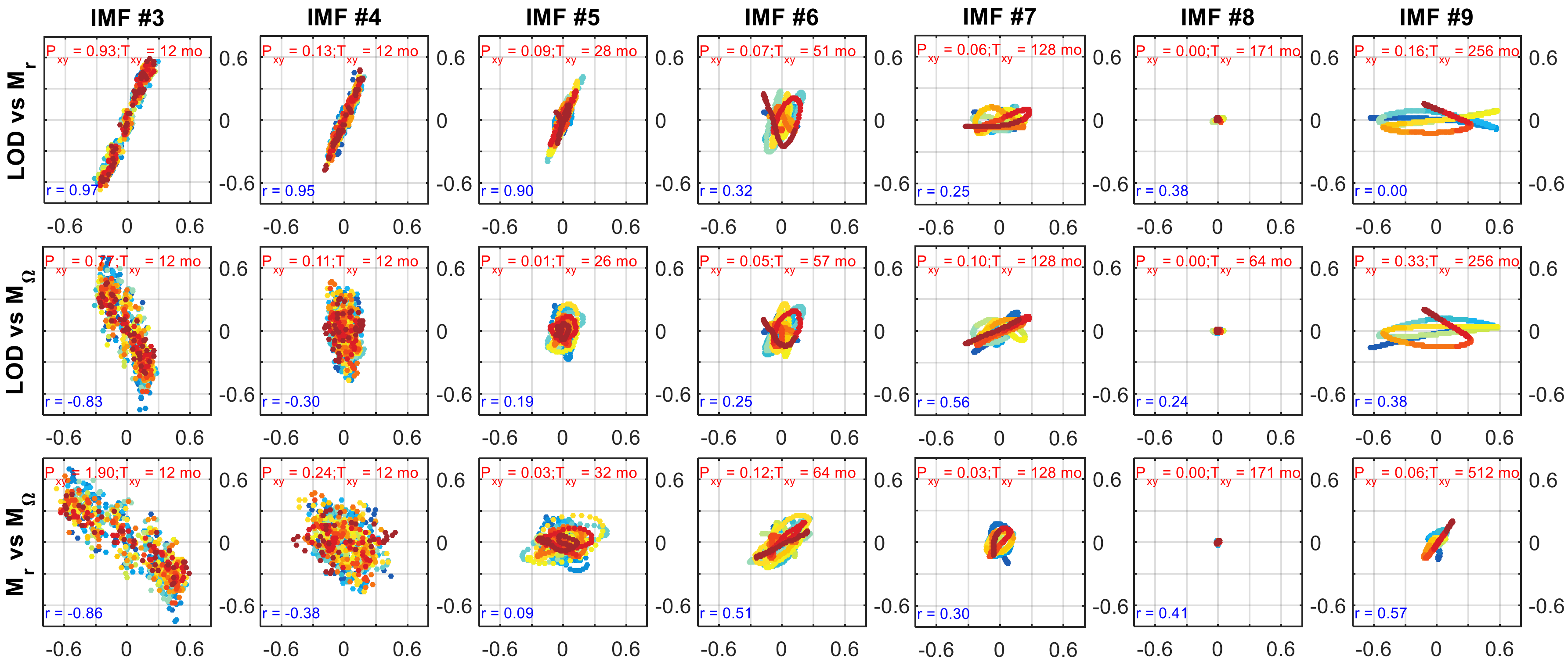

Figure 3. Scatter plots between IMFs resulted from trivariate EMD analysis of normalized M_r,M_Ω, and LOD time series. Spearman's correlation coefficients (r printed in blue) and maximum cross power spectral density (CPSD) along with the corresponding period (P_{xy} and T_{xy} printed in red) are also shown in each panel.

gion should significantly contribute to these low-frequency variations. Thus, it is necessary to analyze the spatio-temporal variations of M_Ω and M_r in more detail, particularly to clarify the role of the equatorial region.

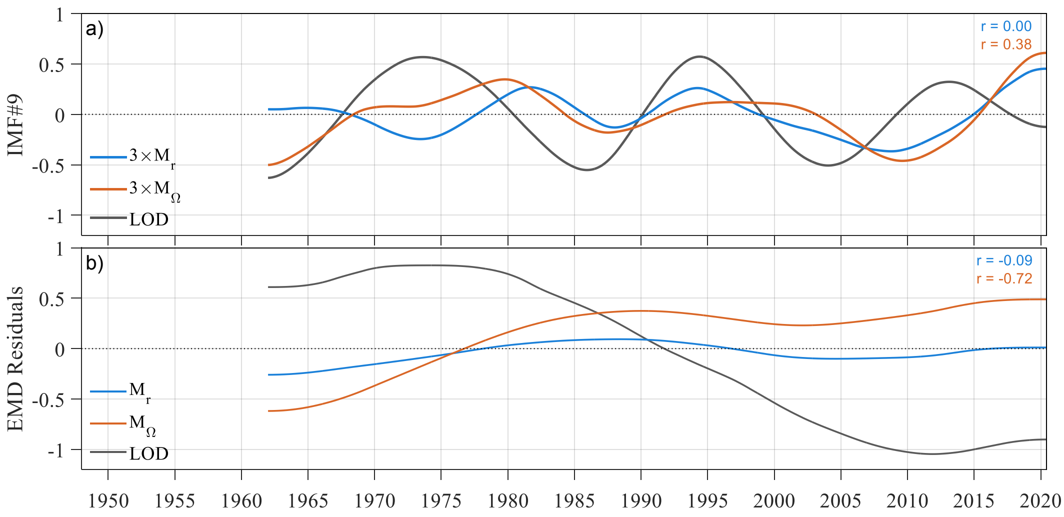

Figure 4. Time series plots of (a)IMFs#9 from Fig. 3 and (b)EMD residuals. Values of IMFs#9 for M_Ω (red lines) and M_r (blue lines) in (a) are multiplied by a factor of 3 for clarity. Correlation coefficients between LOD (black lines) and the other two parameters are shown on the top right corners.

3.2 Spatio-temporal Variations of AAM

Spatial structures of AAM can be obtained by evaluating the integrals in Eqs. (1) and (2) with definite limits for all spatial dimensions (Barnes et al., 1983; Magaña, 1993; Abarca del Rio, 1999; Gong et al., 2019). For example, Eqs. (1) and (2) can be integrated with respect only to longitude and pressure levels to examine latitudinal variations of the AAM. Figures 5(a) and (b) show latitude-time sections of $M_r(\phi)$ and $M_\Omega(\phi)$ anomalies that are calculated as deviations from the climatological (long-term mean) annual-cycle. It can be seen that over the equatorial belt, between 20°S to 20°N, both $M_r(\phi)$ and $M_\Omega(\phi)$ anomalies show a major change from negative to positive values around the 1970s. On the contrary, over the southern midlatitude region between 40°S and 20°S, $M_r(\phi)$ has changed from dominantly positive to more negative values during the same period. In the meantime, the northern midlatitude region between 40°N to 20°N shows more subtle variations.

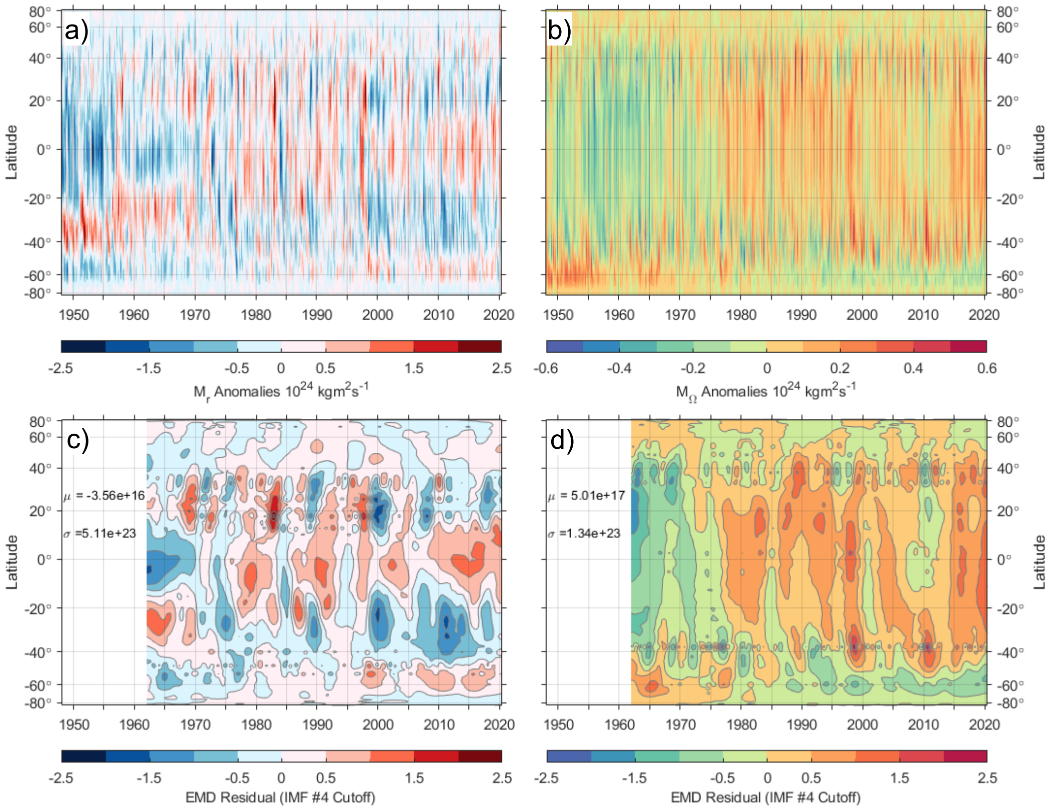

Figure 5. Time-latitude sections of (a)$M_r(\phi)$ anomalies, (b)$M_\Omega(\phi)$ anomalies, (c)EMD residuals of (a), and (d)EMD residuals of (b). EMD residuals are computed with $IMF\#4$ cutoff. Values of mean μ and standard deviation σ used for normalization (see text) are also shown in (c) and (d). Bivariate EMD analyses are performed against the LOD time series so that there is no data before 1962.

To emphasize the temporal and latitudinal structures of low-frequency variations, we applied bivariate EMD analysis on the $M_r(\phi)$ and $M_\Omega(\phi)$ anomalies, shown in Figs. 5(a) and (b), with respect to LOD. In this case, the LOD is not deseasonalized so that all signals are retained in the time series. It should also be noted that, in this implementation of one-dimensional EMD, it is not guaranteed that we can obtain the same maximum number of IMFs for each analysis corresponding to each latitude. However, we found that all time series can be successfully analyzed against LOD up to $IMF\#4$. Therefore, we use this as a cutoff IMF to extract the residuals by Eq. (3) in a manner that is similar to low-pass filtering, whose results are shown in Figs. 5(c) and (d).

The time-latitude sections of residuals in Figs. 5(c) and (d) more clearly show positive trends in both M_r and M_Ω over the equatorial region with patterns of interannual variations that are interwoven across latitudes and throughout the observational period. Other interesting features can be described as follows:

1. As expected from Eq. (2), Figs. 5(d) shows that the equatorial region largely contributes to the changes in $M_\Omega(\phi)$. However, there are extensions or even larger positive changes in either southern or northern midlatitudes during certain periods, such as in the 1990s and most recent decades.
2. There is a negative long-term trend in $M_\Omega(\phi)$ anomalies of higher and polar latitudes of the southern hemisphere, in contrast (but with smaller magnitudes) to the positive trend in the equatorial region.
3. Different from that of $M_\Omega(\phi)$, a contrasting pattern of $M_r(\phi)$ variations are found between the equatorial and southern midlatitude regions, especially in those periods before 1980 and after 2010.
4. Episodes of interannual variations in $M_r(\phi)$ are characterized by propagating patterns, mainly from the equatorial to mid-latitude regions. For example, marked southward (northward) propagation of alternating positive and negative anomalies in the southern (northern) hemisphere can be seen between 1980 and 1990 (1985 and 1995).

As shown in Fig. 5, we can identify the important contribution of the equatorial atmosphere to the variations of global AAM. This view is further augmented by Fig. 6, which depicts time-height cross-sections of global (Fig. 6(a)) and equatorial (Fig. 6(c)) M_r anomalies with similar patterns of spatio-temporal variations. In the upper troposphere and lower stratosphere (UTLS), the equatorial QBO dominates although the contribution to the total AAM is limited because of the low density. Through the troposphere, on the other hand, vertically coherent interannual variation prevails with large contribution of the equatorial region. As in Fig. 5, herein, we apply bivariate EMD analysis on $M_r(p)$ and LOD to obtain the residuals, with $IMF\#4$ cutoff, in each pressure level, and show them in Figs. 6(b) and (d) for global and equatorial regions, respectively. By visual comparisons, the vertical structure of global $M_r(p)$ anomalies is largely characterized by the variations in the equatorial region. In addition, we delineate three layers where $M_r(p)$ variations are significantly different, i.e., the lower troposphere (1000 to 700 hPa), the mid and upper troposphere (700 to 250 hPa), and UTLS (250 to 10 hPa). By focusing on the low-frequency variations of equatorial $M_r(p)$ in Figs. 6(d), temporal structures in these three layers can be described as follows:

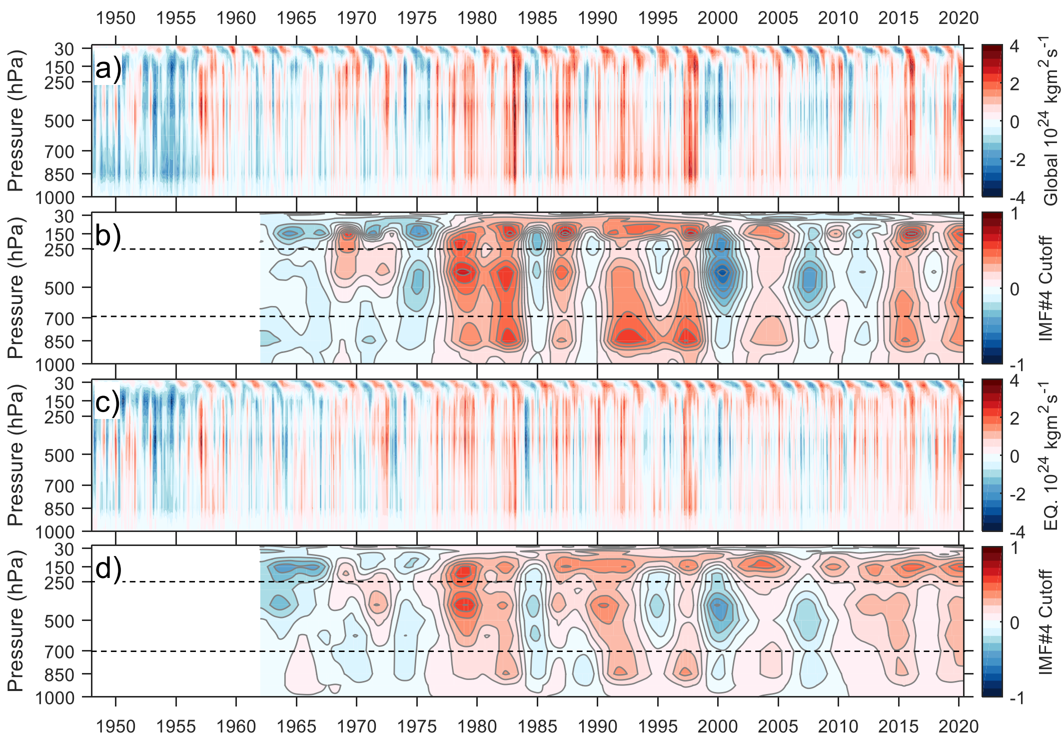

Figure 6. Similar to Fig. 5 but for time-vertical sections of $M_r(p)$: (a)global (pole-to-pole) anomalies, (b)EMD residuals of (a), (c)equatorial (20°S to 20°N) anomalies, and (d)EMD residuals of (c). Data for EMD analyses are normalized using σ in Fig. 5(c) as a common denominator, whereas mean values are computed and subtracted to the time series for each layer. Horizontal black dashed lines mark three divisions of vertical layers, which are further analyzed in Fig 7.

1. Overall, $M_r(p)$ anomalies have drastically changed from predominantly negative before the mid 1970s to mostly positive in all layers after 2010.
2. In UTLS, $M_r(p)$ anomalies are characterized with one major change from dominantly negative to dominantly positive values in the mid-1970s.
3. In the mid and upper troposphere layer, more significant positive and negative variations of $M_r(p)$ occurred between 1975 to 2010, transitioning into a deep layer of positive anomalies that are more pronounced in the last decade.
4. In the lower troposphere layer, $M_r(p)$ variations are characterized by alternating in- and out-of-phase changes with respect to those in the middle and upper tro-

posphere before 2000; since then, these variations have been more consistently in-phase.

3.3 Low-Frequency Variations of Equatorial AAM

It is still difficult to see whether these changes are vertically propagating downward or upward from the previously mentioned results. However, it is interesting to examine further the correlations among low-frequency variations of equatorial M_r in the previously mentioned three layers and LOD. Therefore, we again apply bivariate EMD analysis between layer-averaged M_r and LOD and plotted the residuals, but with $IMF\#6$ cutoff, in Fig. 7. It can be seen that in these residuals, LOD variations are characterized by a three-peak pattern that occurred around the 1970s, 1990s, and 2010s, superimposed on a long-term negative trend. On the other hand, M_r variations differ from one layer to the other with a less discernible positive trend except in UTLS (Fig. 7(a)).

In Fig. 7, we also calculated and plotted Earth's acceleration (black dashed lines), which is simply defined as the negative time derivative of LOD residuals (black lines), i.e.,

$$\dot{\Lambda} = -\frac{d\Re_{LOD}}{dt} \tag{4}$$

If LOD excitation is associated with atmospheric variations, $\dot{\Lambda}$ should be proportional to the rate of change of AAM, which also means proportional to total torques that are mainly contributed by the frictional and mountain torques (Gong et al., 2019). All-time correlation coefficients between M_r and normalized $\dot{\Lambda}$ is more than 0.4 in the lower troposphere, whereas those in the other two layers are around 0.3. Computed 20-year sliding correlation coefficients (shown as bar charts) confirm that low-frequency variations of M_r in the lower troposphere are more consistently in phase with $\dot{\Lambda}$. In contrast, changes in the sign of the sliding correlations occur in other layers. These results indicate that more direct interactions between Earth's rotation and AAM occur in the equatorial lower troposphere.

3.4 Long-term Trend of Equatorial AAM

In the previous subsections, we have shown that EMD residuals can be regarded as low-pass filtered time series when cutoff IMF number is not the maximum; otherwise, residuals are more associated with trends (Wu et al., 2007). As shown in Fig. 4(b),

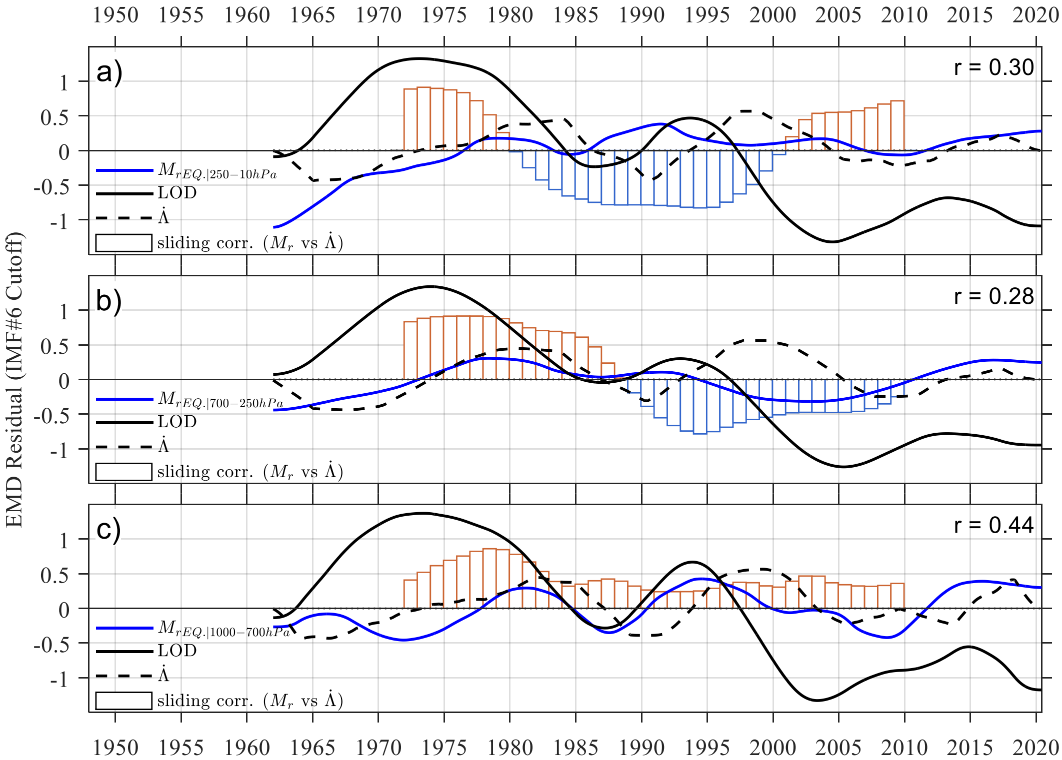

Figure 7. Bivariate EMD residuals with $IMF\#6$ cutoff of LOD (solid black lines) and equatorial M_r (blue lines) averaged in three layers (see Fig. 6): (a)UTLS (250 - 10 hPa),(b)middle and upper-troposphere, and (c)lower troposphere (1000 - 700 hPa). Black dashed lines denote normalized Earth acceleration $\dot{\Lambda}$ defined by equation (4), whereas bar charts depict the coefficients of 20-year sliding correlation between M_r and $\dot{\Lambda}$ (see text).

the long-term trend in LOD is correlated with globally integrated M_Ω rather than M_r. However, since M_Ω is contributed mainly by the equatorial region, we analyzed the trends by focusing on the equatorial atmosphere. The residuals of LOD along with $\dot{\Lambda}$, M_Ω, and lower tropospheric M_r are shown in Fig. 8. It can be seen that a large portion of the LOD time series is monotonically decreasing from around 1980 to around 2010, which is negatively correlated with the long-term trend of M_Ω and M_r over the equatorial region. Although there are still some undulating components in the time series, acceleration in the Earth's rotation during 1970s to 2000 is associated with an increase in M_Ω and lower tropospheric M_r over the equatorial region.

Although the values of M_Ω are determined mainly by surface pressure over the equatorial belt, Fig. 5(d) indicates that there are also temporal variations in midlatitude and

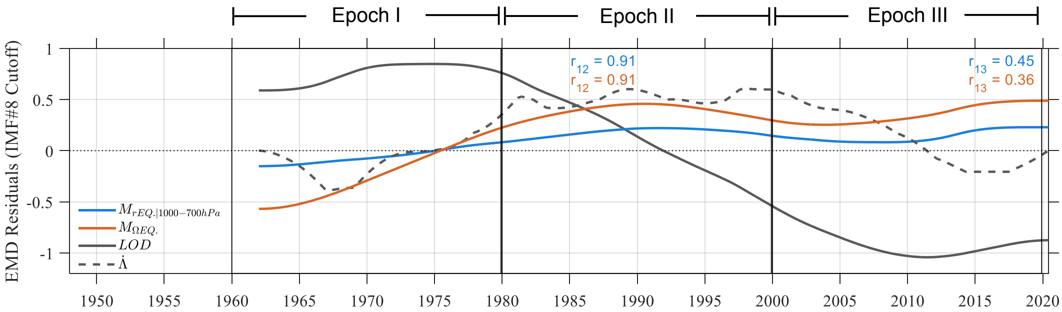

Figure 8. Similar to Fig 4 but for EMD residuals with the largest $IMF\#8$ cutoff showing trends of equatorial lower tropospheric M_r (blue line), M_Ω (red line), and LOD (solid black line), as well as normalized $\dot{\Lambda}$ (black dashed line). The data period is divided into three 20-year epochs, as indicated on the top.

polar regions. To see the horizontal structures of the trends, we divide the data period into three 20-year epochs as indicated on the top of Fig. 8 and plotted the differences in $M_\Omega(\phi,\lambda)$ and lower tropospheric $M_r(\phi,\lambda)$ between two consecutive epochs as colored contour maps in Fig. 9. It can be seen that between the first two epochs, $M_\Omega(\phi,\lambda)$ had almost uniformly increased over the entire equatorial belt, especially over the African and Asian Continents. An increase in $M_\Omega(\phi,\lambda)$ can also be observed over the Maritime Continent and Indian Ocean, whereas the trends in midlatitude regions over the Pacific Ocean are mainly negative. Furthermore, the southern polar region is markedly characterized by negative trends. These trends are largely reversed between the third and second epochs except over the Central Pacific and southern polar region. The magnitude of negative trends between the last two epochs is, in general, weaker compared to the preceding positive trends, but a relatively large decrease in $M_\Omega(\phi,\lambda)$ is observed over the Maritime Continent.

Change of signs also characterizes the trends in lower tropospheric $M_r(\phi,\lambda)$ but with more significant zonal variations along the equatorial belt. Positive trends between the first two epochs mainly occurred over the Pacific Ocean and South America, with contrasting negative trends over the Atlantic Ocean and Africa. This pattern is somewhat reversed from the second and third epochs, with positive trends over the Atlantic Ocean. However, while trends over the Pacific Ocean become negative, positive trends still prevail over the eastern Pacific and South America. Persistent positive trends are also observed over the southern polar region and western part of the Maritime Continent.

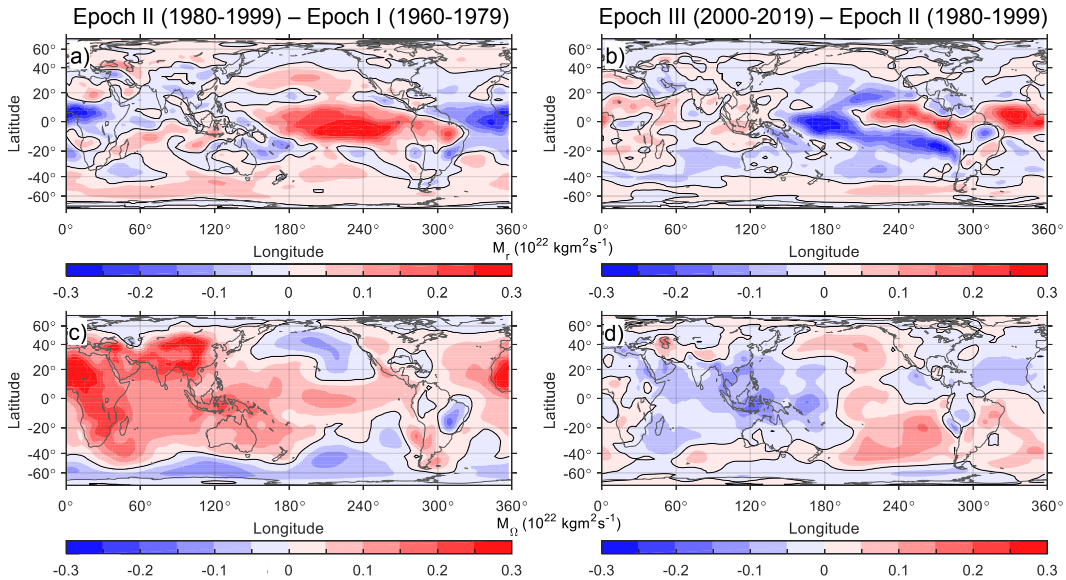

Figure 9. Spatial variations of trends in $M_r(\phi, \lambda)$ (upper panels) and $M_\Omega(\phi, \lambda)$ (lower panels) calculated as differences in mean values between two consecutive epochs defined in Fig. 8.

4 Discussions

Our results of EMD analyses strongly indicate that the increase in Earth's rotation rate during the last five decades can be associated with an increase in both M_Ω and lower tropospheric M_r over the equatorial belt (Fig. 8). The long-term trend of equatorial M_Ω is similar to that of the global domain (Fig. 5 (b)), which is negatively correlated with *LOD* and indicates the important role of equatorial region. Although transient phenomena like MJO and ENSO may have residual effects at longer times (Huang et al., 2001; Lee, 1999), which could be manifested as low-frequency oscillatory variations in Fig. 7, our results are more suggestive that the long-term positive trend in M_Ω found in Fig. 8 was mainly forced by the global increase of surface pressure as indicated by Fig. 9(c). The period around the mid-1970s, during which M_Ω have significantly increased, is widely known as the period of global climate shift event (e.g., Meehl et al., 2009). The positive trend is more relaxed afterward, but the global increase of surface pressure during the 1970s seems to have a prolonged effect on the equatorial M_Ω.

Variations of M_r and M_Ω are, on average, tend to be positively correlated at interannual and longer time scales (Fig. 3). However, positive correlation between M_r and M_Ω only prevails over the equatorial region, whereas negative correlation is more predominant over mid- and high-latitude regions (Figs. 5(c) and (d)). The negative correlation between M_r and M_Ω reflects the AAM conservation and, on the contrary, positive correlation implies residual changes due to acting torques. The increase in equatorial lower-tropospheric M_r should correspond to weaker easterlies, which is explicable by a larger transfer of eastward momentum to the atmosphere due to accelerating Earth (Figs. 7 and 9) but globally integrated M_r shows almost negligibly small long-term trend (Fig. 4). This indicates that spatio-temporal redistribution of M_r anomalies tends to balance residual changes in the equatorial atmosphere. Figure 5 shows that $M_r(\phi)$ anomalies tend to be dominantly negative in midlatitude regions during recent decades, while positive anomalies are stronger near the southern hemispheric polar region. However, this condition is almost the opposite of what has been observed before the mid-1970s, and poleward propagation of $M_r(\phi)$ anomalies can be identified in the interannual variations. Herein, we do not discuss pathways of spatial redistribution of the equatorial $M_r(\phi)$ anomalies in further detail. Among other possibilities, Huang et al. (2003) have studied the transient M_r variations associated with 1965 and 1972 El Niños and Salstein (2015) pointed out that poleward propagation of ENSO induced AAM anomalies has been identified in previous studies.

A long-lasting change in M_Ω might lead to an important impact on the Earth's climate system. In this regard, we have shown a possible connection between M_Ω and LOD, but various Earth-bound and solar-terrestrial processes, including global warming, could be attributable to multidecadal variations in LOD and AAM either dependently or interdependently. However, ocean-atmosphere interactions play major roles in long-term climatic processes. Fig. 9 shows that the multidecadal trends in $M_r(\phi, \lambda)$ exhibit strong zonal variations, indicating different roles of oceans and continents in the momentum transfers along the equatorial region. Considering that the dynamical system of the oceans has longer memory compared to that of the atmosphere, it is quite intuitive to examine correlations between LOD and oceanic climate indices as presented in Fig. 10, where we have chosen three indices to compare with LOD, i.e., Nino34 (ENSO), DMI (Dipole Mode Index), and AMO (Atlantic Multi-decadal Oscillation) index representing oceanic climate variabilities in the Pacific Ocean, Indian Ocean, and the Atlantic Ocean. In addition, GMI (Geomagnetic Ap index) that represents the non-atmospheric/oceanic component is also analyzed. Wahr (1988) pointed out that changes in the Earth's rotation due to electromagnetic forcing are viable.

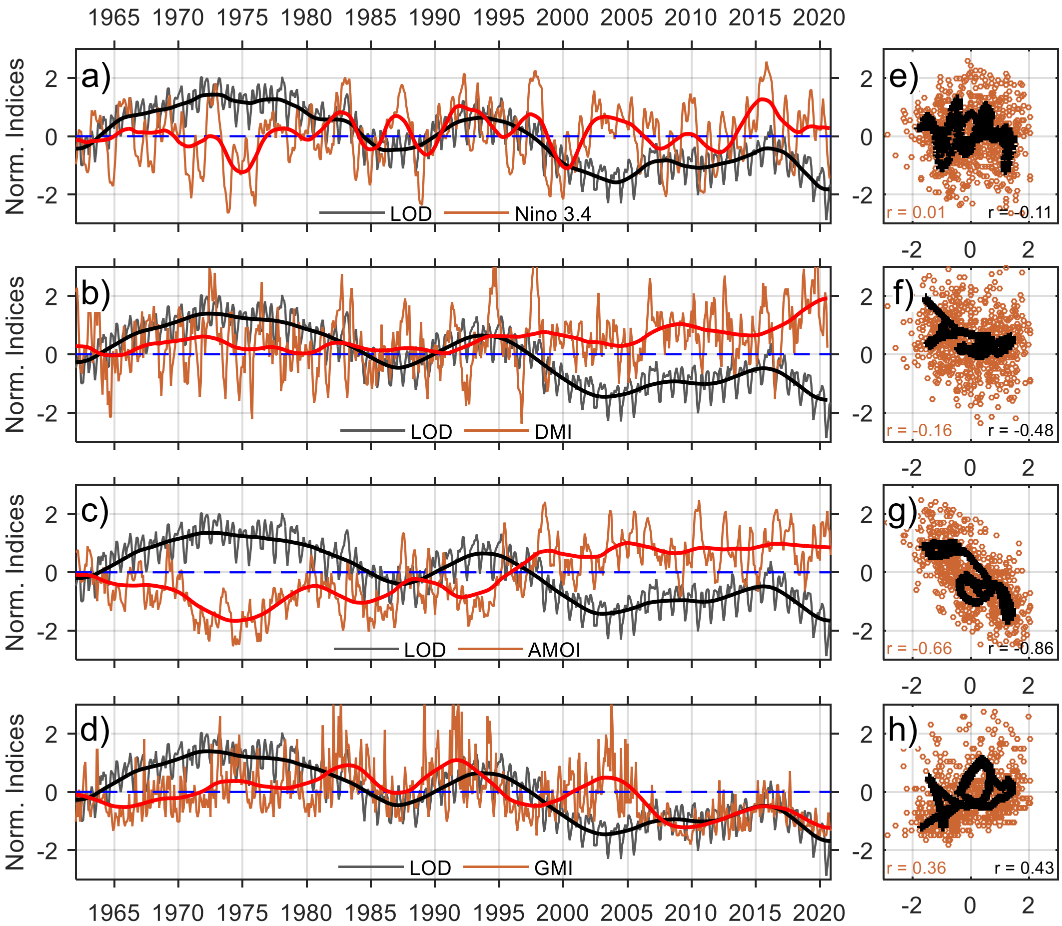

Figure 10. Correlations between *LOD* (black lines) and three oceanic climate indices, i.e., Nino34, DMI, AMO index, and geomagnetic (Ap) index (red lines) presented in the form of time series (left panels) and scatter plots (right panels). Thick lines on the left panels are smoothed values obtained as bivariate EMD residuals with subjectively chosen *IMF#* cutoff. For the scatter plots, red circles and black plus marks correspond to monthly (raw) and smoothed data, respectively. Correlation coefficients are also shown in the scatter plots.

Among four analyzed indices, it is clear from Fig. 10 that AMO has the strongest linear correlation with *LOD*. Even for monthly time series, the correlation between AMO index and *LOD* is around -0.7 and close to -0.9 for the smoothed data. This result somewhat differs from that of Marcus (2016), who found that *LOD* has a stronger correlation with global mean SST than AMO. It is probably also noteworthy that Fig. 10 shows higher negative (positive) correlations between LOD and DMI (GMI) compared to that of LOD and Nino34. Detailed processes that link AMO and other climate indicators with LOD variations are beyond the scope of this study. Nonetheless, we can point out that the Earth's rotation rate is closely related to atmospheric and oceanic variations that define climate conditions at decadal and longer time scales.

5 Conclusions

We have analyzed the low-frequency variability of AAM by applying the bivariate and trivariate EMD method to extract coherent nonstationary signals from the monthly time series of LOD, M_Ω, and M_r, as well as climate indices. We have found that, over the global domain, the decreasing trend of LOD during the last five decades is correlated with an increasing trend in M_Ω, whereas the trend in M_r is negligible.

The long-term positive trend in M_Ω is most likely attributed to a global increase in surface pressure from the mid-1970s until about 1990, which seems to have profoundly affected the atmosphere-ocean dynamical systems over the equatorial belt for a prolonged duration. There is a significant positive trend in M_r of the equatorial lower troposphere (from 1000 to 700 hPa), which is consistent with a larger transfer of eastward momentum due to accelerating Earth. However, a slight long-term trend in globally integrated M_r and spatio-temporal variations of M_r suggest a redistribution of M_r anomalies across the globe by climate processes at interannual to multidecadal time scales.

Although we do not specifically investigate the primary source of low-frequency LOD variations, a comparison between the time series of LOD and the AMO index shows a high correlation coefficient value. Furthermore, we have inferred that two-way interactions between Earth rotation and AAM at a multidecadal time scale are plausible so that changes in Earth's rotation rate are (at least) partially attributable to low-frequency oceanic and atmospheric variability and vice versa. Thus, incorporating a feedback mechanism of LOD variations might need to be considered in future development of global climate models to accurately describe the angular momentum transfer between the solid Earth and the atmosphere and oceans.

Acknowledgments

This research was mainly supported by JSPS-DGHE of The Indonesian Ministry for Education, Culture, Research, and Technology Joint Research Project FY 2020. The first and second authors (TWH and FRF) are also partially supported by ITB-P3MI Research Grant FY 2021.

References

Abarca del Rio, R. (1999). The influence of global warming in earth rotation speed. *Annales Geophysicae*, *17*(6), 806–811. doi: 10.1007/s00585-999-0806-x

Abarca-del Rio, R., Gambis, D., & Salstein, D. (2000, 03). Interannual signals in length of day and atmospheric angular momentum. *Annales Geophysicae*, *18*, 347-364. doi: 10.1007/s00585-000-0347-9

Aoyama, Y., & Naito, I. (2000). Wind contributions to the earth's angular momentum budgets in seasonal variation. *Journal of Geophysical Research: Atmospheres*, *105*(D10), 12417-12431. doi: 10.1029/2000JD900101

Barlyaeva, T., Bard, E., & Abarca-del Rio, R. (2014). Rotation of the earth, solar activity and cosmic ray intensity. *Annales Geophysicae*, *32*(7), 761–771. doi: 10.5194/angeo-32-761-2014

Barnes, R. T. H., Hide, R., White, A. A., & Wilson, C. A. (1983). Atmospheric angular momentum fluctuations, length-of-day changes and polar motion. *Proceedings of the Royal Society of London. Series A, Mathematical and Physical Sciences*, *387*(1792), 31–73.

Birner, T., Davis, S. M., & Seidel, D. J. (2014). The changing width of earth's tropical belt. *Physics Today*, *67*(12), 38-44. doi: 10.1063/PT.3.2620

Bizouard, C., Lambert, S., Gattano, C., Becker, O., & Richard, J.-Y. (2019, 08). The iers eop 14c04 solution for earth orientation parameters consistent with itrf 2014. *Journal of Geodesy*, *93*, 621–633. doi: 10.1007/s00190-018-1186-3

Davis, S. M., & Rosenlof, K. H. (2012). A multidiagnostic intercomparison of tropical-width time series using reanalyses and satellite observations. *Journal of Climate*, *25*(4), 1061 - 1078. doi: 10.1175/JCLI-D-11-00127.1

Duhau, S. (2006). Solar activity, earth's rotation rate and climate variations in the secular and semi-secular time scales. *Physics and Chemistry of the Earth, Parts A/B/C*, *31*(1), 99 - 108. (Long Term Changes and Trends in the Atmosphere) doi: 10.1016/j.pce.2005.03.006

Egger, J., & Hoinka, K.-P. (2005). The annual cycle of the axial angular momentum of the atmosphere. *Journal of Climate*, *18*(6), 757 - 771. doi: 10.1175/JCLI-3290.1

Egger, J., Weickmann, K., & Hoinka, K.-P. (2007). Angular momentum in the global atmospheric circulation. *Reviews of Geophysics*, *45*(4). doi: 10.1029/2006RG000213

Fajary, F. R., Hadi, T. W., & Yoden, S. (2019). Contributing factors to spatiotemporal variations of outgoing longwave radiation (olr) in the tropics. *Journal of Climate*, *32*(15), 4621 - 4640. doi: 10.1175/JCLI-D-18-0350.1

Feldstein, S. B. (1999). The atmospheric dynamics of intraseasonal length-of-day fluctuations during the austral winter. *Journal of the Atmospheric Sciences*, *56*(17), 3043 - 3058. doi: 10.1175/1520-0469(1999)056⟨3043:TADOIL⟩2.0.CO;2

Fujiwara, M., Wright, J. S., Manney, G. L., Gray, L. J., Anstey, J., Birner, T., ... Zou, C.-Z. (2017). Introduction to the sparc reanalysis intercomparison project (s-rip) and overview of the reanalysis systems. *Atmospheric Chemistry and Physics*, *17*(2), 1417–1452. doi: 10.5194/acp-17-1417-2017

Gong, H., Huang, M., Zhu, L., & Shao, Y. (2019). Long-term variations of atmospheric angular momentum and torque. *Meteorology and Atmospheric Physics*, 1-15.

Grimes, A. (1951). Equatorial meteorology. In T. F. Malone (Ed.), *Compendium of meteorology: Prepared under the direction of the committee on the compendium of meteorology* (pp. 881–886). Boston, MA: American Meteorological Society. doi: 10.1007/978-1-940033-70-9_71

Huang, H.-P., Weickmann, K. M., & Hsu, C. J. (2001). Trend in atmospheric angular momentum in a transient climate change simulation with greenhouse gas and aerosol forcing. *Journal of Climate*, *14*(7), 1525 - 1534. doi: 10.1175/1520-0442(2001)014⟨1525:TIAAMI⟩2.0.CO;2

Huang, H.-P., Weickmann, K. M., & Rosen, R. (2003). Unusual behavior in atmospheric angular momentum during the 1965 and 1972 el niños. *Journal of Climate*, *16*, 2526-2539.

IERS Earth Orientation Centre. (2020). *EOP 14 C04 series for 1962-continuing.*

[dataset]. IERS Earth Orientation Centre. Retrieved from https://datacenter.iers.org/data/223/eopc04_14.62-now.txt (Update frequency: bi-weekly)

Kalnay, E., Kanamitsu, M., Kistler, R., Collins, W., Deaven, D., Gandin, L., … Joseph, D. (1996). The NCEP/NCAR 40-Year Reanalysis Project. *Bulletin of the American Meteorological Society*, *77*(3), 437 - 472. doi: 10.1175/1520-0477(1996)077⟨0437:TNYRP⟩2.0.CO;2

Lambeck, K., & Hopgood, P. (1982, 12). The earth's rotation and atmospheric circulation: 1958-1980. *Geophysical Journal International*, *71*(3), 581-587. doi: 10.1111/j.1365-246X.1982.tb02785.x

Lee, S. (1999). Why are the climatological zonal winds easterly in the equatorialupper troposphere? *Journal of the Atmospheric Sciences*, *56*(10), 1353 - 1363. doi: 10.1175/1520-0469(1999)056⟨1353:WATCZW⟩2.0.CO;2

Madden, R. A. (1987). Relationships between changes in the length of day and the 40- to 50- day oscillation in the tropics. *Journal of Geophysical Research: Atmospheres*, *92*(D7), 8391-8399. doi: 10.1029/JD092iD07p08391

Magaña, V. (1993). The 40- and 50-day oscillations in atmospheric angular momentum at various latitudes. *Journal of Geophysical Research: Atmospheres*, *98*(D6), 10441-10450. doi: 10.1029/93JD00343

Marcus, S. (2016). Does an intrinsic source generate a shared low-frequency signature in earth's climate and rotation rate? *Earth Interactions*, *20*, 1-14.

Match, A., & Fueglistaler, S. (2019). The buffer zone of the quasi-biennial oscillation. *Journals of the Atmospheric Sciences*, *76*(11), 3553–3567. doi: 10.1175/JAS-D-19-0151.1

Meehl, G., Hu, A., & Santer, B. (2009). The mid-1970s climate shift in the pacific and the relative roles of forced versus inherent decadal variability. *Journal of Climate*, *22*, 780-792.

NCEP/NWS/NOAA/U.S. Department of Commerce. (1994). *NCEP/NCAR Global Reanalysis Products, 1948-continuing.* [dataset]. NOAA/ESRL/PSL. Retrieved from https://psl.noaa.gov/data/gridded/data.ncep.reanalysis.html

Oort, A. H. (1989). Angular momentum cycle in the atmosphere?ocean?solid earth system. *Bulletin of the American Meteorological Society*, *70*(10), 1231 - 1242. doi: 10.1175/1520-0477(1989)070⟨1231:AMCITA⟩2.0.CO;2

Paek, H., & Huang, H.-P. (2012). A comparison of the interannual variability in atmospheric angular momentum and length-of-day using multiple reanalysis data sets. *Journal of Geophysical Research: Atmospheres*, *117*(D20). doi: 10.1029/2012JD018105

PSL/NOAA. (2020). *Climate Indices.* PSL/NOAA. Retrieved from `https://psl.noaa.gov/data/climateindices/` (Data collected from various sources)

Salstein, D. A. (2015). General circulation of the atmosphere — angular momentum of the atmosphere. In G. R. North, J. Pyle, & F. Zhang (Eds.), *Encyclopedia of atmospheric sciences (second edition)* (Second Edition ed., p. 43-50). Oxford: Academic Press. doi: 10.1016/B978-0-12-382225-3.00043-8

Salstein, D. A., Kann, D. M., Miller, A. J., & Rosen, R. D. (1993). The sub-bureau for atmospheric angular momentum of the international earth rotation service: A meteorological data center with geodetic applications. *Bulletin of the American Meteorological Society*, *74*(1), 67–80.

Starr, V. P. (1948). An essay on the general circulation of the earth5 atmosphere. *Journal of Atmospheric Sciences*, *5*(2), 39 - 43. doi: 10.1175/1520-0469(1948)005⟨0039:AEOTGC⟩2.0.CO;2

Thirumalaisamy, M. (2020, July). *Fast and adaptive multivariate and multidimensional emd.* Retrieved from `https://www.mathworks.com/matlabcentral/fileexchange/71270-fast-and-adaptive-multivariate-and-multidimensional-emd` (MATLAB Central File Exchange)

Thirumalaisamy, M. R., & Ansell, P. J. (2018, Oct). Fast and adaptive empirical mode decomposition for multidimensional, multivariate signals. *IEEE Signal Processing Letters*, *25*(10), 1550-1554. doi: 10.1109/LSP.2018.2867335

Wahr, J. M. (1988). The earth's rotation. *Annual Review of Earth and Planetary Sciences*, *16*(1), 231-249. doi: 10.1146/annurev.ea.16.050188.001311

Weickmann, K. M., & Sardeshmukh, P. D. (1994). The atmospheric angular momentum cycle associated with a madden-julian oscillation. *Journal of Atmospheric Sciences*, *51*(21), 3194 - 3208. doi: 10.1175/1520-0469(1994)051⟨3194:TAAMCA⟩2.0.CO;2

Wu, Z., Feng, J., Qiao, F., & Tan, Z.-M. (2016). Fast multidimensional ensemble empirical mode decomposition for the analysis of big spatio-temporal datasets. *Philosophical Transactions of the Royal Society A: Mathematical, Physical and*

Engineering Sciences, *374*(2065), 20150197. doi: 10.1098/rsta.2015.0197

Wu, Z., Huang, N. E., Long, S. R., & Peng, C.-K. (2007). On the trend, detrending, and variability of nonlinear and nonstationary time series. *Proceedings of the National Academy of Sciences*, *104*(38), 14889–14894. doi: 10.1073/pnas.0701020104

Zotov, L., Bizouard, C., & Shum, C. (2016). A possible interrelation between earth rotation and climatic variability at decadal time-scale. *Geodesy and Geodynamics*, *7*(3), 216-222. (Special Issue: Geodetic and Geophysical Observations and Applications and Implications) doi: 10.1016/j.geog.2016.05.005

Supporting Information for "On the Relationships between Low-Frequency Variations of Earth's Rotation and Equatorial Atmospheric Angular Momentum"

T. W. Hadi[1], F. R. Fajary[1], S. Yoden[2]

[1]Atmospheric Science Research Group, Bandung Institute of Technology, Indonesia

[2]Institute for Liberal Arts and Sciences, Kyoto University, Japan

Contents of this file

1. Figures S1

Introduction

This supporting information provides a figure.

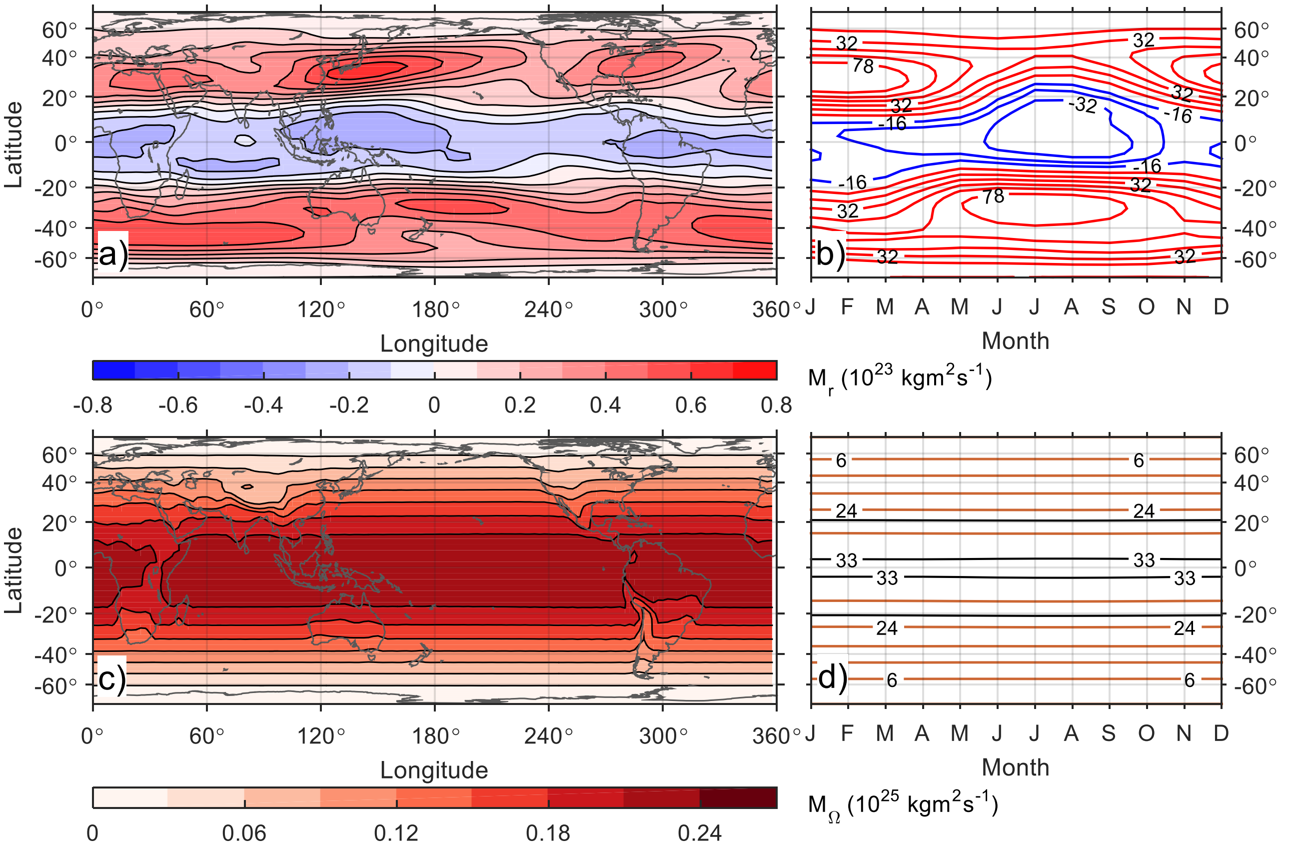

Figure S1. Horizontal distribution of time-averaged (a)$M_r(\phi, \lambda)$ and (c)$M_\Omega(\phi, \lambda)$ components of global AAM. Mean annual variations of longitudinally integrated AAM corresponding to (a) and (c) are depicted as a time-latitude composite in (b) and (d), respectively. The time axis in (b) and (d) shows the months (from January through December). Spatial structures of $M_r(\phi, \lambda)$ and $M_\Omega(\phi, \lambda)$ are computed from NCEP R1 reanalysis zonal wind and surface pressure data by evaluating the integrals in equations (1) and (2) in the paper with definite limits for spatial (ϕ, λ) dimensions.